Pore-Scale Investigation of Uranium Leaching in Low-Grade Rocks via Spectral X-ray Tomography: Evidence for the role of Analcimes in Uranium Mobilization

Maud Herbelin[1*], Ousmane Mangane[2], Stephane Faucher[3], Joseph Diaz[2], Peter Moonen[2,3], Sébastien Hocquet[1], Patrice Creux[2]

1- ORANO, 125 avenue de Paris, 92320 Châtillon, France

2- Université de Pau et des Pays de l'Adour, CNRS, LFCR, 64000 Pau, France

3- Université de Pau et des Pays de l'Adour, CNRS, DMEX, 64000 Pau, France

Abstract: Uranium leaching from ores depends on both pore-scale geometry and mineralogical heterogeneity. While X-ray tomography enables non-invasive characterization of pore morphology and mineral-pore interfaces, we show that conventional tomography cannot unambiguously identify uranium-bearing minerals in low-grade ores because uranium inclusions are smaller than the spatial resolution of the measurements. We propose spectral tomography as an alternative approach and demonstrate that it correctly identifies uranium closely associated to relatively weakly attenuating analcime, whereas highly attenuating features in conventional CT images correspond to barium-bearing phases. These interpretations are independently confirmed by SEM-EDS measurements. A subsequent leaching experiment demonstrates that both morphological and mineralogical changes can be monitored over time. Our results establish spectral tomography as a promising tool for investigating reactive pore-scale processes in ores with complex mineralogy and provide data that can support the optimization of in situ uranium recovery and, more broadly, the extraction of critical mineral resources.

Keywords: In-Situ Recovery; Uranium; Multispectral X-ray tomography; Analcime

1. Introduction

Uranium is among the 60 established Critical Raw Materials (CRM) of the US Department of Energy. More than half of the world's identified recoverable uranium resources are concentrated in three countries: Australia (~28%), Kazakhstan (~14%) and Canada (~10%). Conventional uranium mining involves the extraction of ore, crushing and processing to recover the minerals of interest, while the more recent In-Situ Recovery (ISR)mining method is involving the injection of a leaching solution directly into the deposit, followed by the dissolution of uranium-bearing minerals, the recovery and further purification of the uranium-rich solution at the surface. 2022 represented a tipping point, where more than 50% of the world resources were operated with some ISR Technique (IAEA, 2017). ISR offers multiple advantages compared to classical pit mining, including minimal surface disturbance and the capability to reach deeper zones too complex or expensive to exploit otherwise.

The recovery estimates are performed with reservoir simulators specialized in reactive flow, permitting to optimize the injected and recovery quantities, and to assess the associated risk and environmental impact. These simulators are currently calibrated based on macroscopic experiments on columns (Ben Simon et al., 2014; Bonnet et al., 2024; Dangelmayr et al., 2017; Hoummady et al., 2018). However, the governing processes controlling ISR performance take place at the pore scale: the contact surface between the uranium mineralization and the

accessible pore space, the morphology of the uranium-rich mineral, and the exact mineralogy are examples of very relevant parameters that determine and quantify the reactive flow in porous media (Ben Simon et al., 2014). Whereas contact surface and morphology are geometrical features, the mineralogy defines the solubility. Some kinds of mineralization are poorly soluble, such as Ti-U minerals (Gilligan and Nikoloski, 2015), while for others the solubility may be conditioned by the uranium valence. Uranium IV is, for instance, very weakly soluble for non-extreme pHs and requires oxidation before solubilizing with an acid or an alkali in solution. In contrast, Uranium VI is directly soluble in acid (Bots and Behrends, 2008; Cumberland et al., 2016). Contact between uranium and the acidified solution in the connected pore space is therefore not a sufficient condition to guarantee lixiviation in acid ISR method. In addition, a secondary mineralization may block the flow paths (Mehta et al., 2015; Pan et al., 2016). It appears crucial to be able to visualize the lixiviation process at the pore scale to analyze and quantify the mechanisms, and to improve the calibration of reservoir simulation models for ISR applications.

Among various existing experimental techniques, X-ray microtomography (CT) is of particular interest, as it enables to non-invasively characterize the morphology of representative sample volumes at the pore scale. Moreover, in combination with Hassler or triaxial cells (Azeemuddin et al., 1995; Voltolini et al., 2019), processes can be tracked over time. As an example, a recent study employed CT to investigate the evolution of the pore structure and to determine the reactive transport parameters during acid leaching of sandstone uranium ore (Wang et al., 2024).

Unfortunately, conventional CT does not provide direct chemical information. The complexity of new kinds of deposits such as fractured reservoirs (Jamet et al., 2024), deep (Mkhatshwa et al., 2020), phosphates (Romero Guzmán et al., 1995) or massive ore bodies (Chi et al., 2019; Tschirhart et al., 2022) requires the identification and quantification of the reactive processes. Conventional methods are insufficient to fully understand the complexity of the mechanisms involved.

In the current paper, we explore the potential of spectral X-ray microtomography (sp-CT) to fill this gap. This recent technological development maintains the advantages of conventional CT (non-invasive 3D quantification of pore-scale morphology), but additionally provides element maps (Godinho et al., 2021; Sittner et al., 2021) and mineralogic information (Buyse et al., 2025; Kularatne et al., 2026, 2025). Sp-CT is however not a mature technology yet. The key challenge is to demonstrate that typical Uranium deposits, with concentrations between 100 and 3000 ppm occurring in micrometric structures, can be studied with the current state-of-the-art detectors. This paves the way for the development of experimental setups enabling to perform a comprehensive analysis of the governing pore-scale processing during in-situ leaching.

2. Experimental part

2.1 Rock Sample and Reagents

The investigated rock sample is a uranium-bearing sandstone. Sample machining was carried out in two steps. Two core plugs with a height of 60 and 20 mm and respective diameters of 38 mm and 10 mm were prepared. The remaining annular material was dissolved in concentrated nitric acid and analyzed by ICP-AES to obtain an indicative uranium concentration. The mineral content in uranium was about 830 ppm. One thin section was prepared from one side right next to the small cores taken in order to characterize the mineral composition at the local grain scale with SEM-EDS.

The reagents used include ultrapure water with a resistivity of 18.2 MΩ·cm produced using a THERMO purification system and sulfuric acid (H_2SO_4, >95% purity) obtained from Sigma-Aldrich.

2.2. Experimental Procedure

Pore saturation was achieved using a 30 g/L sulfuric acid solution introduced via vacuum-assisted impregnation. A vacuum pump was used to ensure homogeneous saturation of the porous network. To prevent the retention of solubilized uranium due to gel formation within the pores and to renew the acid, the acid was flushed daily.

2.3 Scanning electron microscopy

Scanning electron microscopy coupled with energy-dispersive X-ray spectroscopy (SEM-EDS) analyses were performed on a carbon coated polished thin section using a ZEISS EVO-MA15 scanning electron microscope equipped with an Oxford Instruments X-Max 150 mm² EDS detector. Analyses were conducted at an accelerating voltage (EHT) of 20 kV and a beam current of 2.0 nA. EDS elemental maps were acquired over selected areas at a resolution of 2 µm/pixel, with a dwell time of 160 µs per pixel. The resulting EDS maps were processed to characterize the spatial distribution of the major elements and to identify the different mineral phases.

2.4 X-ray microtomography

2.4.1 Physical principle

In laboratory X-ray tomography, a sample is placed between a polychromatic X-ray source and a detector. X-rays are attenuated as they pass through the sample, and the transmitted signal is recorded. Conventional detectors integrate the total energy of the incident beam over the full spectrum, providing a single value per detector pixel. Energy-resolved detectors, in contrast, measure the spectrum at a given energy resolution, providing multiple values per pixel. Measurements are acquired for different sample orientations and used to reconstruct a three-dimensional representation of the sample, composed of voxels (the 3D equivalent of pixels).

For conventional detectors, the voxel value corresponds to the reconstructed attenuation coefficient, which reflects the energy-integrated X-ray attenuation. This depends on both the local material composition and density. Consequently, attenuation values alone are generally insufficient to uniquely identify mineral phases, except in simple cases where the number of minerals is limited and their physical or electron densities are sufficiently distinct.

Spectral CT provides additional information by resolving the energy dependence of X-ray attenuation. Each element exhibits a characteristic attenuation spectrum, with absorption edges providing distinctive spectral signatures. The K-edge, for example, corresponds to the ionization of a K-shell electron and occurs at an energy characteristic of the element. At the K-edge, the onset of K-shell photoelectric absorption produces a characteristic discontinuity in the attenuation spectrum.

2.4.2 Image acquisition

Microtomographic imaging was conducted using a TESCAN UniTOM XL Spectral, equipped with a 2856 × 2856 flat panel detector for conventional CT and a cadmium telluride (CdTe) spectral detector for sp-CT. Image reconstruction was performed using the Panthera software suite provided by TESCAN.

Conventional scans were acquired at a tube voltage of 80 kV with a current of 175 µA, yielding a final isotropic voxel size of 7 µm. Total scan time was 184 minutes/sample. The CdTe detector enabled acquisition of X-ray absorption spectra across 140 energy channels covering

a range from 20 to 160 keV, allowing spatially resolved multispectral reconstruction. Acquiring a full 3D data volume with sp-CT would take about 30 times longer than the CT scan. Therefore, this imaging mode was primarily used for 2D regions of interest identified on conventional CT scans before and after leaching, particularly those associated with potentially soluble minerals or secondary mineral precipitation. Each region-of-interest spectral scan took about 20 minutes. The images generated are visualized using Dragonfly software.

3. Results and discussions

3.1 Mineralized Uranium identification

The sample studied is a coarse-grained feldspathic sandstone with siliceous-hematite cement. The grains are poorly sorted, with some very coarse-grained layers. The mineral assemblage consists mainly of quartz, K-feldspars and albite (Figure 1, Figure 2). Accessory minerals are also observed, such as zircon, apatite, monazite, and rutile. As described in the literature, it was subject to several phases of diagenesis, mineralization, and post-diagenesis (Billon, 2014; Mamane Mamadou, 2016). Analcime ($NaAlSi_2O_6 \cdot H_2O$), a sodium-rich zeolite mineral occurs as intraclasts within the pore space and is characterized by a distinctive atoll-like morphology (Figure 1, Figure 2, Figure 3). Harmotome ($Ba_2CaAl_4Si_{12}O_{32} \cdot 12H_2O$), a barium- and calcium-bearing zeolite mineral is found as a late-stage pore-filling cement (Figure 2, Figure 3). The mineralization occurs as acicular urano-titanates (hereafter referred to as U-Ti), with variable amounts of Ca, Si, Fe and Cu and is closely associated to analcime suggesting replacement of the latter (Figure 3).

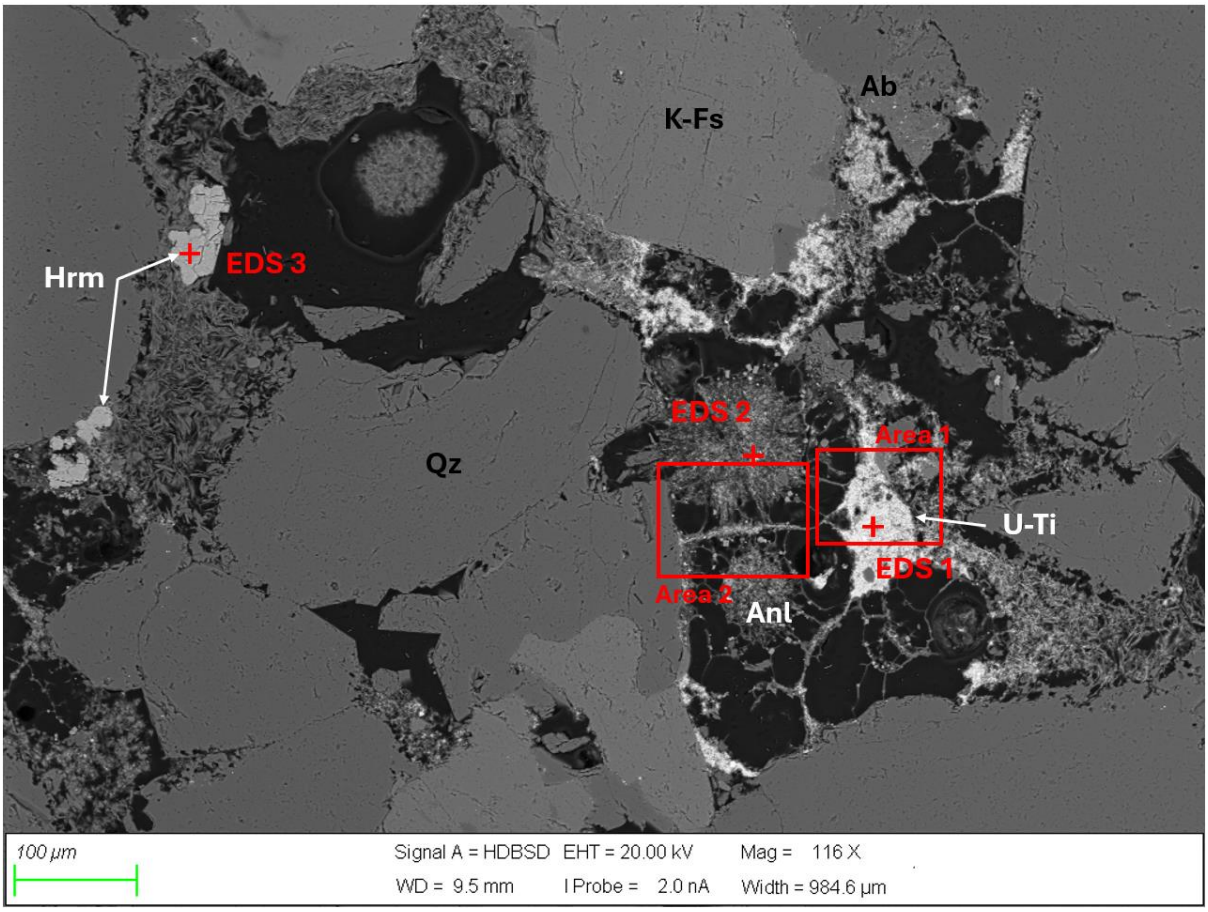

Figure 1: BSE image showing analcime aggregates. Abbreviations: Ab = albite, Anl = analcime, Hrm = harmotome, K-Fs = potassium feldspar, Qz = quartz, U-Ti = urano-titanate.

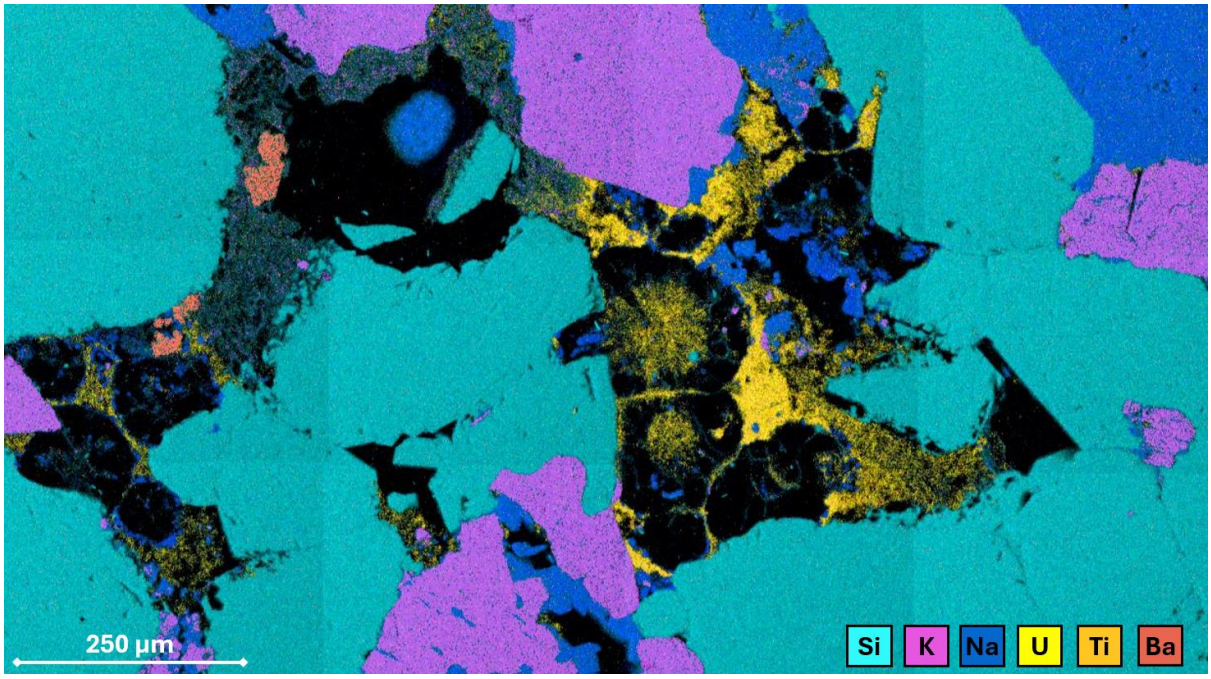

Figure 2: Multielement EDS map for the same area as Figure 1.

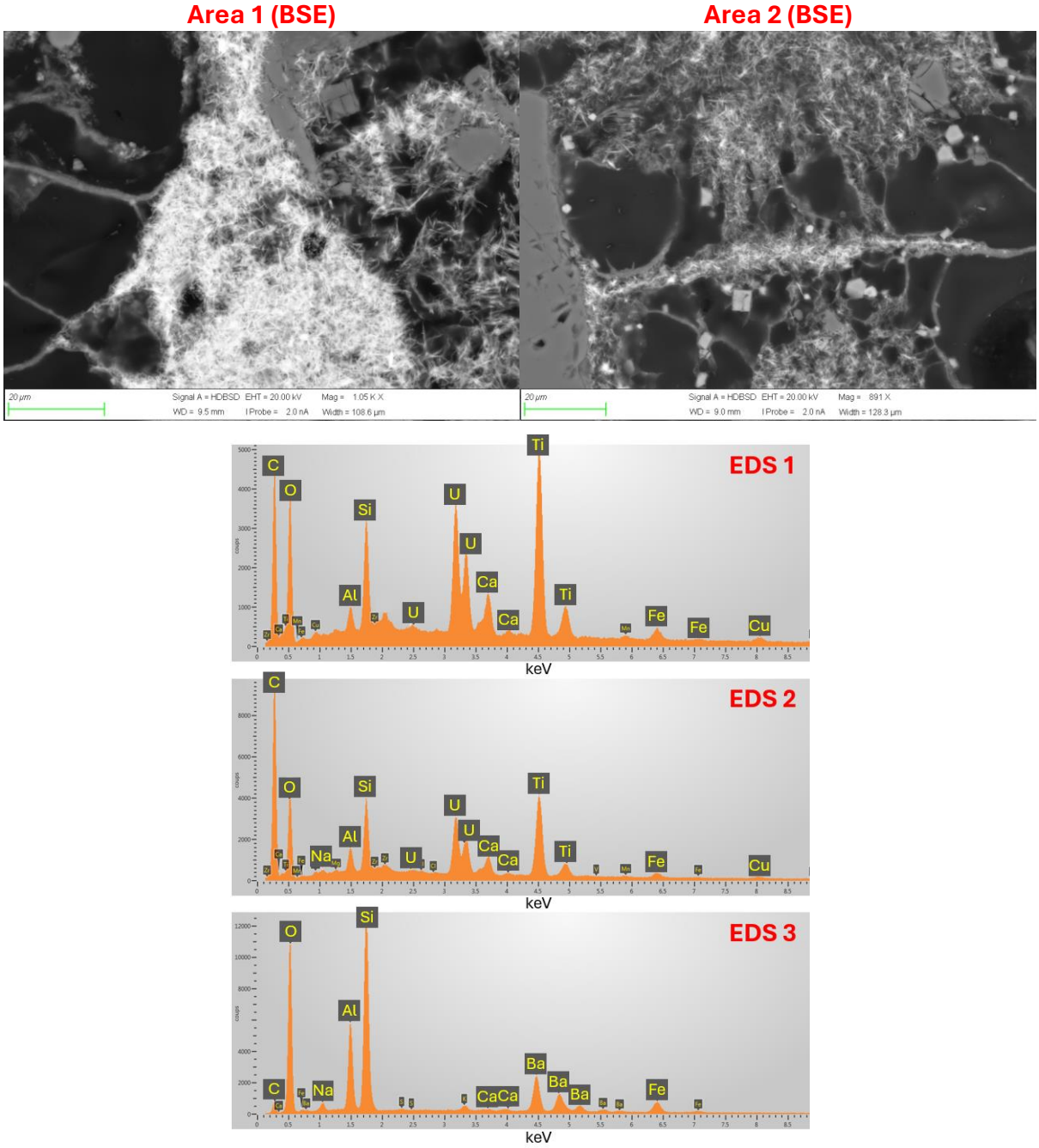

Figure 3: Detailed BSE images and EDS spectra corresponding the analysis points shown in Figure 1. Area 1 : acicular U-Ti ; Area 2 : analcime replacement by U-Ti ; EDS 1 : U-Ti ; EDS 2 : analcime with U-Ti ; EDS 3 : harmotome.

Figure 4a shows a slice through the uranium-containing sample obtained by conventional CT, where the most attenuating structures appear in white. Although uranium is the most attenuating element in the sample (specific gravity ≈ 19; Z = 92), spectral CT (Figure 4b) shows that the brightest regions are associated with barium-rich structures, characterized by a K-edge around 40 keV. In contrast, the uranium K-edge at 115 keV is detected in regions appearing darker in the conventional CT image (Figure 4a–b).

This apparent discrepancy results from the small size of the uranium-bearing particles, i.e. below the voxel size. Their attenuation is therefore averaged with that of the surrounding minerals, preventing reliable phase segmentation at the uranium concentrations investigated. Higher spatial resolution could improve uranium detection, but only over smaller sample

volumes, limiting representativeness. Spectral CT therefore provides a means of localizing uranium phases at representative sample dimensions.

SEM-EDS analyses confirmed that the most attenuating minerals are harmotome (Figure 1, Figure 3). In contrast, petrographic and geochemical analyses indicate that analcime-rich horizons host uranium, with analcime locally replaced by urano-titanates. Analcime may also incorporate trace amounts of uranium, mainly as uranyl species (UO_2^{2+}), through cation-exchange processes. Its negatively charged framework provides sorption sites that can retain uranium within its microporous structure and influence U mobility in surrounding pore fluids (Bonnet et al., 2024).

Although analcime is not a primary uranium host, its presence and partial replacement by urano-titanates may influence the distribution and retention of uranium under variable redox conditions. These features should therefore be considered in reactive transport modelling and geochemical assessments of uranium-bearing sedimentary rocks (Jamet et al., 2024).

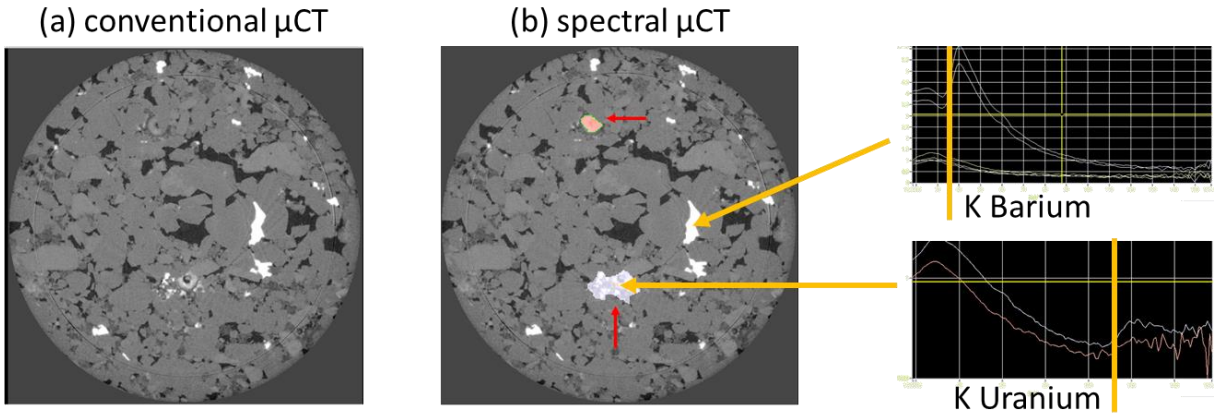

Figure 4: Cross-sectional slice through the sample, obtained with conventional X-ray tomography (1a) and spectral X-ray tomography (1b). The figures on the right correspond to the detected attention curves of the mineral indicated by the arrows.

3.2 Mobilization of the Uranium

The stability of the X-ray source and low detector noise ensure consistent data acquisition under identical conditions (voxel size, voltage, and current), allowing reliable comparison of the sample before and after successive leaching cycles. Figure 5 shows four regions of interest before and after leaching. A progressive darkening of the images is generally observed, consistent with uranium dissolution from the core across different geological structures. However, given the low uranium content at the voxel scale, neither conventional nor spectral tomography allows accurate local quantification. In addition, analcime can incorporate a range of heavy elements, meaning that changes in grey level cannot be unambiguously attributed to uranium dissolution at the scale of observation.

Analcime ($NaAlSi_2O_6 \cdot H_2O$), can strongly influence fluid–rock interactions through its cation-exchange capacity and reactivity under acidic conditions. Its negatively charged aluminosilicate framework is balanced by exchangeable extra-framework cations, mainly Na^+, which can readily participate in ion-exchange reactions (Liu et al., 2025; Novembre and Gimeno, 2021; Sakizci, 2016).

Under acidic conditions (pH < ~4–5), such as those encountered during sulfuric acid leaching in ISR, H^+ competes with Na^+ for exchange sites, promoting Na^+/H^+ exchange and proton consumption (Parrotin et al., 2024). Acidic conditions can also promote partial dissolution of the aluminosilicate framework through proton-promoted hydrolysis of Si–O–Al bonds

(Hartman and Fogler, 2006). Together, these processes can modify the availability of exchange sites and promote the release of previously sorbed species.

Under oxidizing conditions, uranium occurs predominantly as aqueous U(VI), mainly as uranyl (UO_2^{2+}). Although direct evidence for uranyl incorporation into analcime remains limited, its well-established ion-exchange behavior suggests that UO_2^{2+} may be transiently retained on exchange sites or surfaces, particularly in Na-rich pore fluids. Acidification would favor competitive proton exchange and promote uranyl release. Proton-promoted dissolution may further contribute to U remobilization by exposing new reactive surfaces and releasing incorporated species.

Once released, U(VI) remains soluble under sulfuric acid leaching conditions, where sulfate complexes such as $UO_2SO_4^0$ and $UO_2(SO_4)_2^{2-}$ can enhance its transport. The combined effects of ion exchange and partial mineral dissolution therefore provide a plausible mechanism for uranium mobilization in analcime-bearing sandstones. Our images show that acid reaches uranium-bearing regions associated with analcime and urano-titanates, although no significant dissolution of the analcime structure is observed after acid contact. This suggests that uranium can be accessed during leaching without requiring extensive dissolution of the analcime host structure.

At the reservoir scale, these coupled processes may affect both uranium recovery and petrophysical properties. Analcime dissolution may modify porosity and permeability, while ion exchange can alter fluid chemistry and buffering capacity. These processes should therefore be considered in reactive transport models of ISR of the studied site.

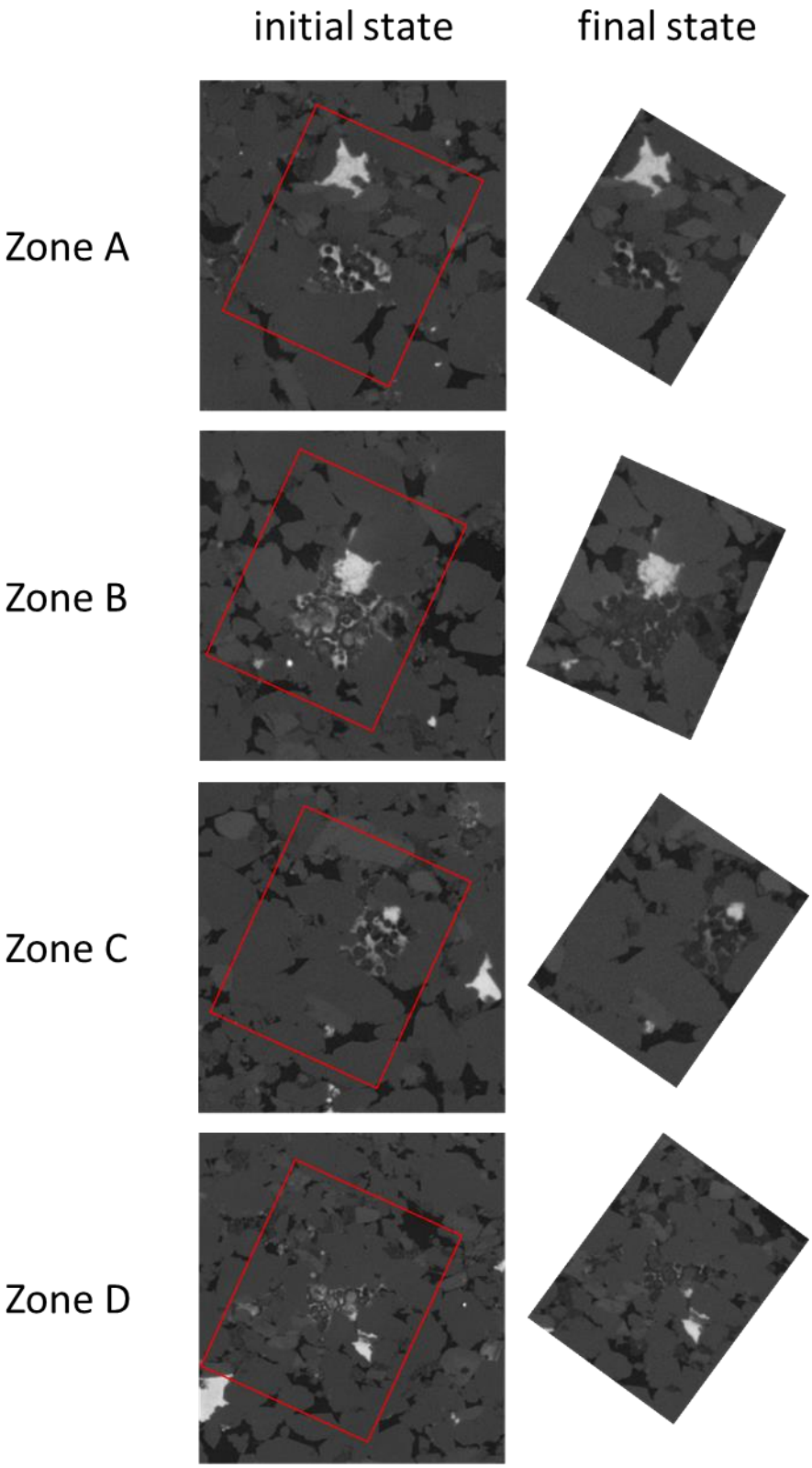

Figure 5 : Four zones of interest based on microtomography images showing uranium dissolution for 4 different analcime aggregates (left: initial state t = 0, right: final state t = 6 days).

4. Conclusions

Mining investments, particularly in the uranium sector, are steadily increasing due to the exploitation of deeper and more geologically complex formations, coupled with increasingly stringent environmental regulations. In Situ Recovery (ISR) techniques have emerged as a key

method to access low grade, heterogeneous and complex mineralization. Given the strategic importance of uranium for nuclear energy, these developments are central to the transition toward low-carbon energy systems. The technical and environmental viability of ISR projects relies on advanced reservoir modeling, at all phases of the project, from planning, over production up to site rehabilitation. Accurate models are essential not only for predicting resource recovery, but also for minimizing environmental impacts and supporting the sustainable extraction of critical raw materials.

In this context, we present a novel approach for studying ISR processes at representative uranium concentrations. By integrating spectral X-ray microtomography with pore-scale imaging, this method enables the direct identification of uranium traces and the monitoring of their dissolution during leaching. This approach provides unique insights into the microscale mechanisms governing ISR performance and brings a 3D chemical analysis visualizing uranium content and leading to decisive information linked to the access to the mineralization.

Acknowledgements

We thank the funding support from the Agence Nationale de la Recherche (ANR) (ANR-24-CHIN-0009) and ORANO as part of the SATURNE chair program.

References

Azeemuddin, M., Roegiers, J.-C., Suri, P., Zaman, M., Kukreti, A.R., 1995. Stress-dependent permeability measurement of rocks in a triaxial cell, U.S. Rock Mechanics/Geomechanics Symposium.

Ben Simon, R., Thiry, M., Schmitt, J.-M., Lagneau, V., Langlais, V., Bélières, M., 2014. Kinetic reactive transport modelling of column tests for uranium In Situ Recovery (ISR) mining. Appl. Geochem. 51, 116–129. https://doi.org/10.1016/j.apgeochem.2014.09.014

Billon, S., 2014. Minéraux argileux dans le gisement uranifère d'Imouraren (Bassin de Tim Mersoï, Niger) : implications sur la genèse du gisement et sur l'optimisation des processus de traitement du minerai (Doctorat ès Terre solide et enveloppes superficielles, PhD). Poitiers. https://doi.org/10.70675/277b1b43z9474z4f46zb099z39f6bd999322

Bonnet, M., Robin, V., Parrotin, F., Grozeva, N., Seigneur, N., Batbaatar, M.-E., Descostes, M., 2024. Influence of clay minerals on pH and major cation concentrations in acid-leached sands: Column experiments and reactive-transport modeling. J. Contam. Hydrol. 264, 104363. https://doi.org/10.1016/j.jconhyd.2024.104363

Bots, P., Behrends, T., 2008. Uranium mobility in subsurface aqueous systems: the influence of redox conditions. Mineral. Mag. 72, 381–384. https://doi.org/10.1180/minmag.2008.072.1.381

Buyse, F., Boone, M.N., Van Assche, F., Faucher, S., Moonen, P., Dewaele, S., Cnudde, V., 2025. Spectral X-ray computed tomography for the chemical identification of critical minerals. Tomogr. Mater. Struct. 8, 100059. https://doi.org/10.1016/j.tmater.2025.100059

Chi, G., Chu, H., Petts, D., Potter, E., Jackson, S., Williams-Jones, A., 2019. Uranium-rich diagenetic fluids provide the key to unconformity-related uranium mineralization in the Athabasca Basin. Sci. Rep. 9, 5530. https://doi.org/10.1038/s41598-019-42032-0

Cumberland, S.A., Douglas, G., Grice, K., Moreau, J.W., 2016. Uranium mobility in organic matter-rich sediments: A review of geological and geochemical processes. Earth-Sci. Rev. 159, 160–185. https://doi.org/10.1016/j.earscirev.2016.05.010

Dangelmayr, M.A., Reimus, P.W., Wasserman, N.L., Punsal, J.J., Johnson, R.H., Clay, J.T., Stone, J.J., 2017. Laboratory column experiments and transport modeling to evaluate retardation of uranium in an aquifer downgradient of a uranium in-situ recovery site. Appl. Geochem. 80, 1–13. https://doi.org/10.1016/j.apgeochem.2017.02.018

Gilligan, R., Nikoloski, A.N., 2015. The extraction of uranium from brannerite – A literature review. Miner. Eng. 71, 34–48. https://doi.org/10.1016/j.mineng.2014.10.007

Godinho, J.R.A., Westaway-Heaven, G., Boone, M.A., Renno, A.D., 2021. Spectral Tomography for 3D Element Detection and Mineral Analysis. Minerals 11, 598. https://doi.org/10.3390/min11060598

Hartman, R.L., Fogler, H.S., 2006. The Unique Mechanism of Analcime Dissolution by Hydrogen Ion Attack. Langmuir 22, 11163–11170. https://doi.org/10.1021/la061576q

Hoummady, E., Golfier, F., Cathelineau, M., Truche, L., Durupt, N., Blanvillain, J.-J., Neto, J., Lefevre, E., 2018. An integrated multiscale approach to heap leaching of uranium-ore agglomerates. Hydrometallurgy 178, 274–282. https://doi.org/10.1016/j.hydromet.2018.05.011

IAEA, 2017. In Situ Leach Uranium Mining, IAEA Nuclear Energy Series No. NF-T-1.4. IAEA, Vienna.

Jamet, M., Ballas, G., Soliva, R., Gerbeaud, O., Lefebvre, T., Leredde, C., Loggia, D., 2024. Naturally fractured reservoir characterisation in heterogeneous sandstones: insight for uranium in situ recovery (Imouraren, Niger). Solid Earth 15, 895–920. https://doi.org/10.5194/se-15-895-2024

Kularatne, K., Beaudoin, N.E., Sénéchal, P., Moonen, P., Youssef, S., Nader, F.H., 2025. Pioneering data on detection, identification and quantification of key carbonate minerals using spectral tomography. Mar. Pet. Geol. 182, 107536. https://doi.org/10.1016/j.marpetgeo.2025.107536

Kularatne, K., Darouich, O., Sénéchal, P., Moonen, P., Derluyn, H., 2026. Laboratory spectral X-ray tomography for the differentiation of common rock-forming minerals. Sci. Rep. 16, 20053. https://doi.org/10.1038/s41598-026-47955-z

Liu, J., Ta, A.T., Seaton Ullberg, R., Hounfodji, J.W., Badawi, M., Zur Loye, H.-C., Phillpot, S.R., 2025. Energetics and kinetics of alkali ion exchange in analcime. Phys. Chem. Chem. Phys. 27, 25512–25523. https://doi.org/10.1039/D5CP02373D

Mamane Mamadou, M., 2016. Le système métallogénique des gisements d'uranium associés à la faille d'Arlit (Bassin de Tim Mersoï, Niger) : diagenèse, circulations des fluides et mécanismes d'enrichissement en métaux (U, Cu, V) (Doctorat ès Géosciences, PhD). Université de Lorraine. https://doi.org/10.70675/985bf2bazabedz4d28z924fz7d6661cca41c

Mehta, V.S., Maillot, F., Wang, Z., Catalano, J.G., Giammar, D.E., 2015. Transport of U(VI) through sediments amended with phosphate to induce in situ uranium immobilization. Water Res. 69, 307–317. https://doi.org/10.1016/j.watres.2014.11.044

Mkhatshwa, S.F., Guy, B.M., Smith, A.J.B., Viljoen, K.S., 2020. A mineralogical perspective on the recovery of uranium from brannerite-rich ore at Cooke Section, West Rand

Goldfield, South Africa. South Afr. J. Geol. 123, 615–632. https://doi.org/10.25131/sajg.123.0031

Novembre, D., Gimeno, D., 2021. Synthesis and characterization of analcime (ANA) zeolite using a kaolinitic rock. Sci. Rep. 11, 13373. https://doi.org/10.1038/s41598-021-92862-0

Pan, Z., Giammar, D.E., Mehta, V., Troyer, L.D., Catalano, J.G., Wang, Z., 2016. Phosphate-Induced Immobilization of Uranium in Hanford Sediments. Environ. Sci. Technol. 50, 13486–13494. https://doi.org/10.1021/acs.est.6b02928

Parrotin, F., Dazas, B., Billon, S., Chedozeau, R., Savoye, S., Descostes, M., Tertre, E., 2024. Role of zeolite content on the sorption properties of analcime-rich rocks from the Abinky Formation (Niger). Sci. Total Environ. 925, 171615. https://doi.org/10.1016/j.scitotenv.2024.171615

Romero Guzmán, E.T., Solache Ríos, M., Iturbe García, J.L., Ordoñez Regil, E., 1995. Uranium in phosphate rock and derivates. J. Radioanal. Nucl. Chem. Artic. 189, 301–306. https://doi.org/10.1007/BF02042609

Sakizci, M., 2016. INVESTIGATION OF THERMAL AND STRUCTURAL PROPERTIES OF NATURAL AND ION-EXCHANGED ANALCIME. ANADOLU Univ. J. Sci. Technol. - Appl. Sci. Eng. 17, 724–724. https://doi.org/10.18038/aubtda.266863

Sittner, J., Godinho, J.R.A., Renno, A.D., Cnudde, V., Boone, M., De Schryver, T., Van Loo, D., Merkulova, M., Roine, A., Liipo, J., 2021. Spectral X-ray computed micro tomography: 3-dimensional chemical imaging. X-Ray Spectrom. 50, 92–105. https://doi.org/10.1002/xrs.3200

Tschirhart, V., Potter, E.G., Powell, J.W., Roots, E.A., Craven, J.A., 2022. Deep Geological Controls on Formation of the Highest-Grade Uranium Deposits in the World: Magnetotelluric Imaging of Unconformity-Related Systems From the Athabasca Basin, Canada. Geophys. Res. Lett. 49, e2022GL098208. https://doi.org/10.1029/2022GL098208

Voltolini, M., Barnard, H., Creux, P., Ajo-Franklin, J., 2019. A new mini-triaxial cell for combined high-pressure and high-temperature *in situ* synchrotron X-ray microtomography experiments up to 400°C and 24 MPa. J. Synchrotron Radiat. 26, 238–243. https://doi.org/10.1107/S1600577518015606

Wang, S., Lian, M., Ding, D., He, G., Fu, H., 2024. Evolution of pore structure and reactive transport parameters during acid leaching of sandstone uranium ore. Hydrometallurgy 226, 106301. https://doi.org/10.1016/j.hydromet.2024.106301